Crystal direction dependence of quantum confinement effects of two-dimensional Si layers fabricated on silicon-on-quartz substrates: modulation of phonon spectra and energy band structures

2014 Jpn. J. Appl. Phys. 53 04EC09

(http://iopscience.iop.org/1347-4065/53/4S/04EC09)

Japanese Journal of Applied Physics **53**, 04EC09 (2014) **REGULAR PAPER**
http://dx.doi.org/10.7567/JJAP.53.04EC09

Crystal direction dependence of quantum confinement effects of two-dimensional Si layers fabricated on silicon-on-quartz substrates: modulation of phonon spectra and energy band structures

Tomohisa Mizuno[1]*, Yuhsuke Nagata[1], Yuhya Suzuki[1], Yuhta Nakahara[1], Yoshiki Nagamine[1], Kengo Saita[1], Takashi Aoki[1], and Toshiyuki Sameshima[2]

[1]*Department of Science, Kanagawa University, Hiratsuka, Kanagawa 259-1293, Japan*
[2]*Department of Engineering, Tokyo University of Agriculture and Technology, Koganei, Tokyo 184-8588, Japan*
E-mail: mizuno@info.kanagawa-u.ac.jp

Received September 16, 2013; revised November 15, 2013; accepted November 19, 2013; published online February 13, 2014

We experimentally studied the crystal direction dependence of phonon confinement effects (PCEs) and bandgap (E_G) modulation of a two-dimensional (2D) Si layer fabricated on (100) silicon-on-quartz (SOQ) wafers without a handle Si substrate. For the first time, by polarization Raman spectroscopy, in the case of Raman intensity spectra in the asymmetrical broadening region owing to the PCEs in the 2D Si layer, we demonstrated that the incident laser polarization direction dependence of the Raman intensity deviates from the Raman selection rule. However, a photoluminescence (PL) method shows that the E_G expansion is isotropic in the 2D Si layer. On the other hand, the reflectivity of the 2D Si layer in UV region is also modulated. The reflectivity property modulation is possibly attributable to the energy band modulation in the 2D Si layer.

1. Introduction

Two-dimensional (2D) Si structures are widely used for extremely thin silicon-on-insulator (ETSOI) field-effect transistors (FETs) and 3D metal–oxide–semiconductor (MOS) devices, such as FinFETs,[1)] as well as Si photonic devices.[2,3)] In addition, the surface orientation engineering[4)] and strain technique[5)] have been the major technologies for realizing high-performance CMOS devices. To improve the short-channel effects (SCEs) of MOSFETs and the photoluminescence (PL) intensity I_{PL} of Si photonic devices, the 2D Si thickness T_S should continue to be scaled down.[1–3)] However, the quantum confinement effects (QCEs) in a thinner T_S structure cause electron mobility modulation,[6–8)] which is due to the QCEs of 2D electrons in ETSOIs. In addition, the QCEs induce band structure modulation (BSM), resulting in the band gap E_G expansion of ETSOIs.[9–11)]

Phonon confinement effects (PCEs),[12–18)] which are due to the quantum phonon wave vector uncertainty Δq due to Heisenberg's uncertainty principal, are reported to be enhanced in 1D and 0D Si semiconductors, such as Si nanowires (1D)[13,18)] and nanocrystals (0D),[13,17)] compared with those in ETSOIs, because Δq increases with decreasing Si dimension from 2D to 0D. In the case of 2D Si, the finite Si thickness T_S causes the phonon wave vector uncertainty Δq_L in the longitudinal direction of the 2D Si layer, that is, $\Delta q_L \approx 1/T_S$. As a result, PCEs also occur even in 2D Si. Therefore, the PCEs induce the carrier mobility reduction due to the enhanced phonon scattering of carriers even in ETSOIs.[19)] Moreover, the drain current drivability of 2D Si devices is also degraded by self-heating effects in ETSOI structures, because of the high heat resistance of the buried oxide layer (BOX) in ETSOIs.[1)] Therefore, it is very important to study 2D phonon properties as well as modulated band structures in a 2D Si layer, to clarify both the phonon induced carrier velocity reduction and the modulation of thermal properties (such as thermal conductivity) of 2D Si structures. Recently, we have experimentally demonstrated the asymmetrical broadening and peak downshift of Raman intensities due to PCEs even in (100) and (110) 2D Si with $T_S \approx a$ fabricated by the thermal oxidation process of SOIs,[20,21)] where a is a Si lattice constant of 0.543 nm. PCEs are independent of the surface orientation and tensile strain.[21)]

On the other hand, the QCEs are reported to modulate the 2D Si band structures, and thus, to change the Si crystals to a direct band-gap material from an indirect band-gap 3D Si material.[3,9,19,22)] In particular, it is also reported that the PL peak photon energy E_{PH} increases with decreasing T_S, which is caused by the direct optical transmission in the direct bandgap thin-film Si material that is changed from an indirect bandgap bulk Si material.[21)] On the other hand, we cannot detect the PL intensity from the (110) 2D Si layer, which is probably attributable to the indirect band-gap structure of the (110) 2D Si layer.[21)]

Moreover, the other optical properties of 2D Si layer, such as the relaxation effect of the Raman selection rule (RSR)[23)] caused by PCEs[18)] and the reflectivity modulation caused by the band structure modulation in the 2D Si layer, have not yet been studied in detail, because the optical intensities from the Si substrate under the BOX are relatively higher than those of the thinner 2D Si layer surface. In addition, we have not verified whether the BSM depends on the crystal direction of the 2D Si layer. Therefore, it is strongly required to study the QCE of the 2D Si layer without a handle Si substrate to observe the optical properties of the 2D Si layer directly.

In this work, we experimentally studied the crystal direction dependence of the PCEs and BSM of 2D Si layer formed on (100)-surface silicon-on-quartz (SOQ) wafers without a handle Si substrate under the BOX.[24)] Using a polarization Raman method,[25)] for the first time, we demonstrated that the Raman intensity of the 2D-SOQ in the asymmetrical broadening region deviates from the RSR. On the other hand, we found that the PL peak energy E_{PH}, that is, E_G, is independent of the crystal direction in the 2D-SOQ. We also successfully demonstrated the reflectivity R modulation of the 2D-SOQ, which is enhanced by decreasing T_S. These optical property modulations are considered to be attributable to the BSM in the 2D Si layer.

2. Experimental procedure for 2D Si layers on SOQ

(100) 2D-SOQ was fabricated by a thermal oxidation (Dry-O_2) of (100)-SOQ[26] at a high temperature (1000 °C). Thus, we can directly measure the optical properties (such as R) of 2D Si layer in detail because of the absence of the handle Si substrate beneath the BOX layer. As a reference, 2D Si layer on (100) bonded SOI substrates[27] was also fabricated. The T_S of 2D Si layer is mainly evaluated using a UV/visual reflection spectrum, and the T_S value was also verified by high-resolution transmission electron microscopy (HRTEM).[20,21] In this study, we successfully formed 0.5-nm-thick 2D-SOQ as well as 0.5-nm-thick 2D Si layer on SOI, which have good crystal quality and uniform layers.[20]

We measured the crystal direction dependences of PCEs and BSM by polarization methods, i.e., laser wavelength 442 nm Raman spectroscopy using a He–Cd laser and PL method with an excitation laser photon energy $h\nu$ (h is the Planck constant and ν is the photon frequency) of 2.33 eV (532 nm wavelength) at room temperature, respectively, where the laser power is 1 mW to inhibit the laser-power-induced heating effects of the 2D Si layer[21] and the laser beam diameter is 1 μm. Moreover, we compared 442 nm Raman spectroscopy data with usual 325 nm Raman spectroscopy data.[21] On the other hand, we evaluated the reflectivity R of 2D-SOQ as a function of $h\nu$ in the UV region, where the beam diameter is 1 mm.

3. Results and discussion

3.1 PCEs in 2D-SOQ

Figure 1(a) shows the 442 nm Raman spectrum of 2D-SOQ with $T_S \approx 1$ nm. We experimentally confirmed the asymmetrical broadening of the Raman spectrum even in the 442 nm Raman spectroscopy of 2D-SOQ. To analyze the asymmetrical broadening of the Raman spectrum due to PCEs,[20,21] we introduce the asymmetrical broadening parameters W_L and W_H, as shown in Fig. 1(a). W_L and W_H are the full width at 1/10 maximum (FWTM) of the Raman intensity I_R in the lower and higher wave number regions from 520 cm^{-1} of the first-order Raman scattering of the Γ point in 3D-Si, respectively.[21] Figures 1(b) and 1(c) show the Si atom layer number N_L ($\equiv 4T_S/a + 1$)[21] dependences of W_L and W_H, respectively, where N_L instead of T_S is the best indicator for evaluating PCEs in the 2D Si layer.[21] Here, SOI data were also evaluated by 325 nm Raman spectroscopy. When $N_L < 30$, the W_L of 2D-SOQ rapidly increases with decreasing N_L and exhibits the same N_L dependence of W_L as that of 325 nm Raman spectra of both SOQ and SOI. On the other hand, W_H, which is an indicator of crystalline quality,[21] exhibits almost the same N_L dependence of all data and good crystal quality with the low value in $N_L > 8$. Consequently, the Raman properties of SOQ are the same as those of SOI and independent of the incident laser wavelength less than 442 nm. Thus, hereafter, we used 442 nm Raman spectroscopy data for evaluating the Raman selection rule of 2D-SOQ.

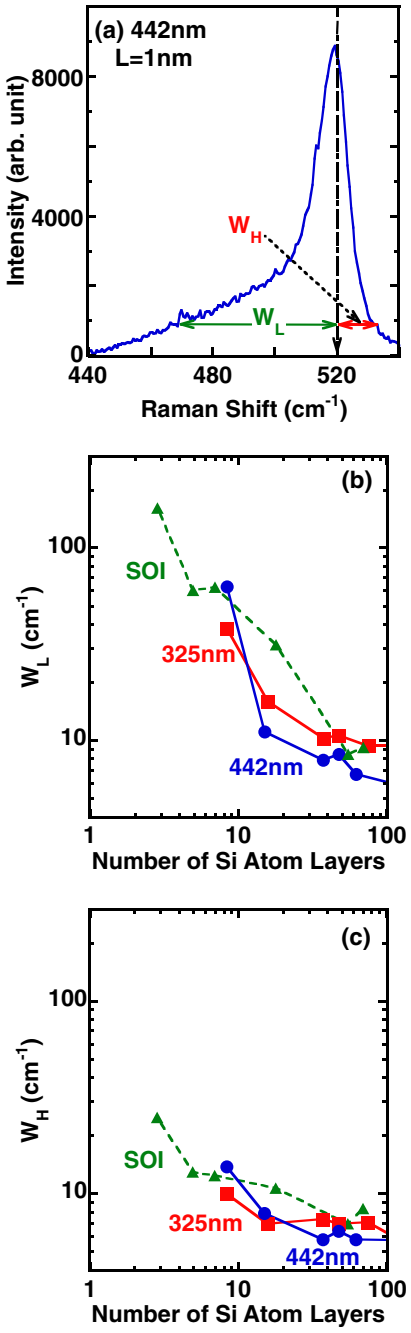

Fig. 1. (Color online) (a) 442 nm laser wavelength Raman spectra of 2D-SOQ with $T_S \approx 1$ nm. Even in 442 nm Raman spectroscopy data, we can observe an asymmetrical broadening of the Raman peak caused by PCEs, similarly that observed in 325 nm Raman spectroscopy data. W_L and W_H are defined by FWTM of the Raman peak intensities in the lower and higher wave number regions from 520 cm^{-1} of the Γ point in the Brillouin zone, respectively. N_L dependence of (b) W_L and (c) W_H of SOQ (squares) and SOI (triangles) evaluated by 325 nm Raman spectroscopy. Circles also show the 442 nm Raman spectroscopy data of SOQ. Almost all data have the same N_L dependence. Therefore, we can evaluate the PCEs of 2D-SOQ in detail using the 442 nm Raman spectroscopy.

3.2 Relaxation of Raman selection rule in 2D-SOQ

The Δq in the 2D Si layer causes the relaxation of the momentum conservation of $\boldsymbol{q}$. As a result, the RSR,[23] which is based on the momentum conservation of $\boldsymbol{q}$ at $\boldsymbol{q} \approx 0$, is also relaxed by Δq. Therefore, Δq causes not only the asymmetrical broadening effects of the Raman spectrum but also the deviation effects from the RSR. We have already demonstrated the Δq induced asymmetrical broadening effects of the Raman spectrum in 2D Si layer.[20,21] However, we have not yet demonstrated the relaxation of the RSR. Thus, in this section, the relaxed RSR in the 2D Si layer is verified using the polarization Raman method.

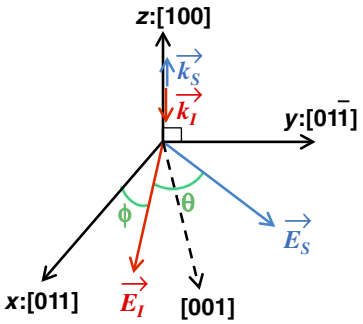

Fig. 2. (Color online) Raman scattering geometry on (100) 2D Si surface. The [100] axis (z-axis) shows the surface orientation of the 2D-Si plane. $\boldsymbol{k}_\mathrm{I}$ is the incident laser vector on the (100) 2D Si layer, and $\boldsymbol{E}_\mathrm{I}$ is the polarization laser vector. The angle between $\boldsymbol{E}_\mathrm{I}$ and the [011] axis in the 2D-Si plane is ϕ. On the other hand, $\boldsymbol{k}_\mathrm{S}$ is the scattered Raman photon vector, and $\boldsymbol{E}_\mathrm{S}$ is the polarization Raman photon vector with the angle θ between $\boldsymbol{E}_\mathrm{I}$.

Figure 2 shows the Raman scattering geometry on a (100) 2D Si surface with the Raman scattering vector ($\boldsymbol{k}_\mathrm{S}$) of the z-axis and an incident laser beam vector ($\boldsymbol{k}_\mathrm{I}$) on (100) 2D Si layer. When the polarization laser vector and polarization Raman vector are $\boldsymbol{E}_\mathrm{I}$ and $\boldsymbol{E}_\mathrm{S}$, respectively, ϕ is the angle between the x-axis of the crystal direction [011] and $\boldsymbol{E}_\mathrm{I}$, and θ is the angle made by $\boldsymbol{E}_\mathrm{I}$ and $\boldsymbol{E}_\mathrm{S}$. As a result, the Raman intensity I_R can be determined by the RSR.[23] Namely,

$$I_\mathrm{R} \propto \sum_J |\boldsymbol{E}_\mathrm{I}\boldsymbol{R}_J\boldsymbol{E}_\mathrm{S}|^2, \tag{1}$$

Here, $\boldsymbol{R}_J$ is the Raman tensor of phonon J for 3D-Si, which is given

$$R_x = \begin{pmatrix} 0 & 0 & 0 \\ 0 & 0 & d \\ 0 & d & 0 \end{pmatrix}, \quad R_y = \begin{pmatrix} 0 & 0 & d \\ 0 & 0 & 0 \\ d & 0 & 0 \end{pmatrix},$$
$$R_z = \begin{pmatrix} 0 & d & 0 \\ d & 0 & 0 \\ 0 & 0 & 0 \end{pmatrix}, \tag{2}$$

where d is a component of $\boldsymbol{F}_{2\mathrm{g}}$ symmetry.[23]

In the case of (100) 3D-Si, I_R can be simply expressed as[23]

$$I_\mathrm{R} \propto \cos^2(2\phi + \theta). \tag{3}$$

Figures 3(a) and 3(b) show experimental polarization Raman spectra of 2D-SOQ with T_S of 1 nm as a function of θ at $\phi = 0°$ ($\boldsymbol{E}_\mathrm{I}$ of [011]) and ϕ at $\theta = 0°$ (parallel to $\boldsymbol{E}_\mathrm{I}$), respectively. DL shows the minimum cutting-off Raman intensity obtained using the Raman polarization filter in this study. Figure 3(a) shows that the Raman intensity at 520 cm^{-1} is nearly equal to the DL level at $\theta = 90°$, as expected, but that the Raman intensities in an asymmetrical broadening region lower than 520 cm^{-1} are much higher than the DL level. Moreover, Fig. 3(b) also shows that the Raman intensity at 520 cm^{-1} rapidly decreases with increasing ϕ, as expected from Eq. (3). However, the Raman intensities in the asymmetrical broadening region still remain finite with values higher than the DL level even at $\phi = 45°$. Therefore, the results shown in Figs. 3(a) and 3(b) obtained in the asymmetrical broadening region are considered to be caused by the relaxation effects of the RSR due to PCEs.[18]

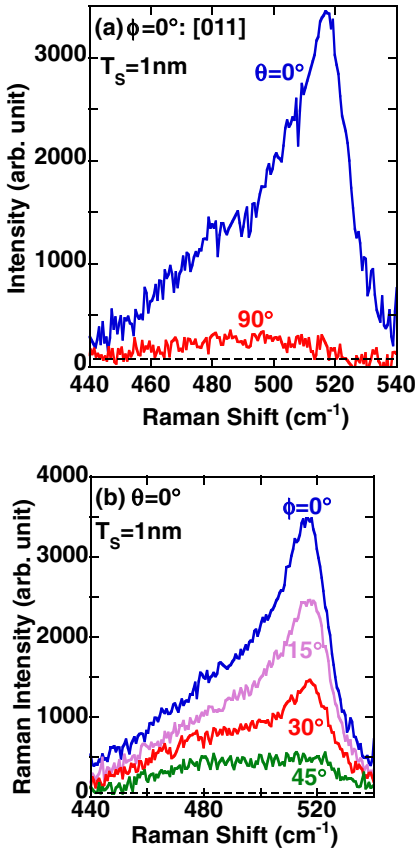

Fig. 3. (Color online) Polarization 442 nm Raman spectra of 2D-SOQ as a function of (a) θ at $\phi = 0°$ ($\boldsymbol{E}_\mathrm{I} = [011]$) and (b) ϕ at $\theta = 0°$ (parallel to $\boldsymbol{E}_\mathrm{I}$), where $T_\mathrm{S} \approx 1$ nm. The dashed line shows the detection limit (DL) for the polarization Raman system in this study. (a) shows that the Raman intensities at 520 cm^{-1} is nearly equal to the DL level at $\theta = 90°$, but that in an asymmetrical broadening region lower than 520 cm^{-1} is much higher than the DL level. Moreover, (b) shows that the Raman intensity at 520 cm^{-1} gradually decreases with increasing ϕ. However, the Raman intensities in the asymmetrical broadening region are still finite with values higher than the DL level even at $\phi = 45°$.

Here, to confirm the relaxation effects of the RSR of Eq. (3) in 2D-SOQ, the ϕ dependence of $I_\mathrm{R}(\phi, \theta)$ was investigated, as shown in Fig. 4, where circles and squares show the $I_\mathrm{R}(\phi, \theta)$ data obtained at $\theta = 0$ and 90°, which are normalized by the maximum $I_\mathrm{R}(\phi, \theta)$ value at the same θ values, respectively. The dashed and dotted lines indicate the theoretical results obtained using Eq. (3) at $\theta = 0$ and 90°, respectively. Figures 4(a) and 4(b) show the experimental ϕ dependence of the $I_\mathrm{R}(\phi, \theta)$ of both 56 nm thick SOQ and 1 nm thick 2D-SOQ at the first-order Raman scattering of 520 cm^{-1}, respectively. It is clear that the ϕ dependence of the I_R of both 56 nm SOQ and 1 nm 2D Si layer can be explained by the theoretical $\cos^2(2\phi + \theta)$ dependence of Eq. (3). Therefore, in this study, we experimentally verified the RSR of 520 cm^{-1} in both 3D- and 2D-SOQ. However, Fig. 4(c) shows that the $I_\mathrm{R}(\phi, \theta)$ of 1 nm 2D-SOQ in the asymmetrical broadening region of 480 cm^{-1} deviates from the $\cos^2(2\phi + \theta)$ dependence of Eq. (3) at both θ values. This ϕ uncertainty $\Delta\phi$ at approximately $\theta = 0$ and 90° becomes approximately 15°, compared to Eq. (3), and this $\Delta\phi$ is attributable to phonon wave vector uncertainty Δq. Thus, for the first time, we experimentally verified that the Δq of PCEs

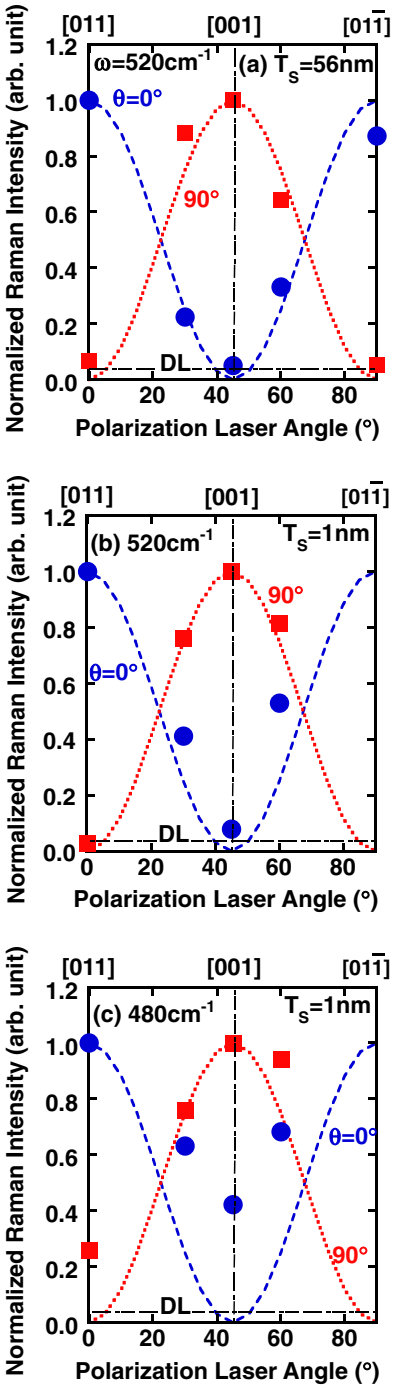

Fig. 4. (Color online) Polarization laser direction ϕ dependence of polarization 442 nm Raman intensity normalized by the peak Raman intensity at the same θ for (a) 520 cm^{-1} peak at $T_S = 56$ nm, (b) 520 cm^{-1} peak at $T_S \approx 1$ nm, and (c) 480 cm^{-1} of PCEs region at $T_S \approx 1$ nm. Circles and squares show the data obtained at $\theta = 0$ and 90°, respectively. The dashed ($\theta = 0°$) and dotted ($\theta = 90°$) lines show the theoretical results of the $\cos^2(2\phi + \theta)$ dependence of Raman intensity obtained using Eq. (3).[23] The Raman intensities at 520 cm^{-1} are almost consistent with the theoretical results, but those at 480 cm^{-1} widely deviate from the theoretical results.

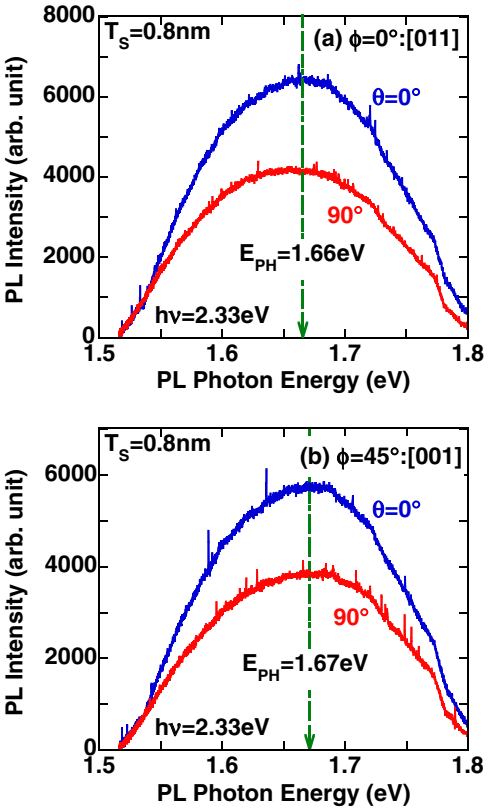

Fig. 5. (Color online) Polarization PL spectra of (a) $\phi = 0°$ ($\boldsymbol{E}_I = [011]$) and (b) $\phi = 45°$ ($\boldsymbol{E}_I = [001]$), where $T_S \approx 0.8$ nm and excitation photon energy $h\nu = 2.33$ eV. Arrows show the peak PL photon energy E_{PH}. E_{PH} is independent of the laser polarization direction, whereas the PL intensity depends on θ.

relaxes the RSR in the asymmetrical broadening region of Raman spectra in the 2D Si layer.

3.3 Crystal direction dependence of band structure modulation in 2D-SOQ

Using the polarization PL method, we studied the crystal direction dependence of E_G characteristics of 2D-SOQ evaluated using the peak PL photon energy E_{PH}. It is expected that the E_G of 2D Si layer will be independent of the crystal direction at the 2D Si layer surface, that is, 2D Si layer has an isotropic E_G, because electrons are confined only in the direction perpendicular to the 2D Si layer.

Figures 5(a) and 5(b) show the polarization PL spectra of 2D-SOQ at $\phi = 0°$ ([011] direction) and 45° ([001] direction), respectively, where $T_S \approx 0.8$ nm. At both ϕ values, we experimentally confirmed the same E_{PH} value of 1.66 eV of 0.8 nm 2D-SOQ in both directions perpendicular and parallel to the incident laser polarization direction. In addition, the E_{PH} of SOQ is the same as that of 0.8-nm 2D-SOI.[21] However, the PL intensity I_{PL} is polarized, because the I_{PL} at the polarization angle $\theta = 0°$ is higher than that at $\theta = 90°$ at both ϕ values.

Here, Figs. 6(a) and 6(b) show the ϕ dependences of E_{PH} and peak I_{PL}, respectively, where $T_S \approx 0.8$ nm, at $\theta = 0°$ (circles) and 90° (squares). Figure 6(a) indicates that E_{PH} values are completely independent of the crystal direction of ϕ and the PL polarization angle of θ, as expected. Therefore, the isotropic E_{PH} shows an isotropic E_G of the 2D Si layer in this study. Moreover, Fig. 6(b) shows that the peak I_{PL} is almost independent of ϕ. Here, the PL polarization P of the peak I_{PL} is defined by $P \equiv (I_{PL0} - I_{PL90})/(I_{PL0} + I_{PL90})$,[28,29] where I_{PL0} and I_{PL90} are the peak I_{PL}'s at $\theta = 0$ and 90°, respectively. It is clear that the PL intensity is polarized in the entire crystal direction, but P is almost independent of ϕ, and the average P is only 0.052 in this study. Therefore, in the

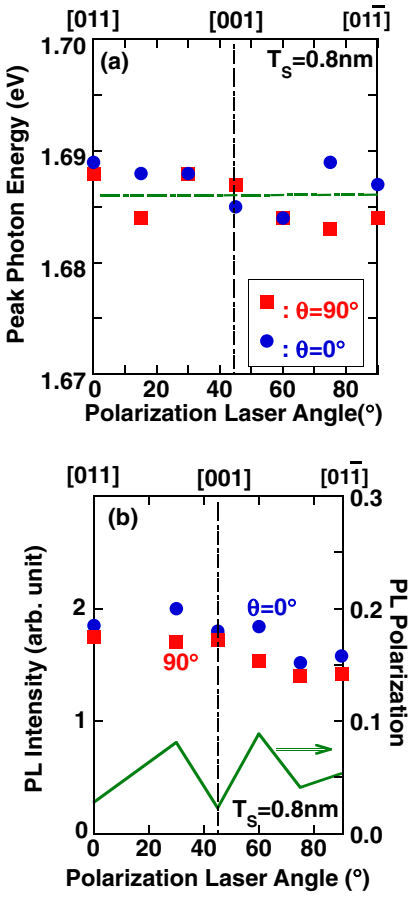

Fig. 6. (Color online) Excitation laser angle ϕ dependences of (a) E_{PH} and (b) I_{PL}, where $T_S \approx 0.8$ nm and $h\nu = 2.33$ eV. (a) shows that E_{PH} is independent of ϕ and θ, which indicates that 2D Si layer has an isotropic E_G value. Moreover, (b) shows mostly an isotropic-I_{PL} at both θ values. The PL polarization shown in the right axis is almost constant (>0) and the average is about 0.052, which shows that I_{PL} at $\theta = 0°$ is slightly higher than that at $\theta = 90°$.

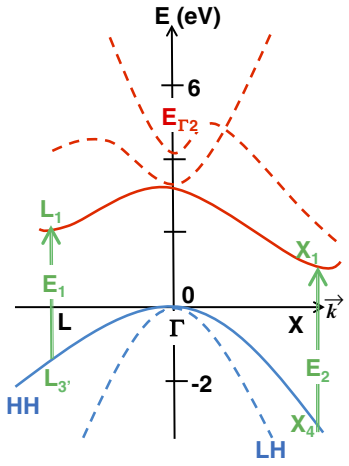

Fig. 7. (Color online) Schematic energy band structures in conduction E_C and valence bands of 3D-Si as a function of electron wave vector $\boldsymbol{k}$ (transverse axis), where HH and LH are the heavy and light hole bands, respectively. Using high energy photons in the UV region, electrons can directly transit from the $L_{3'}$ level of the HH level to the L_1 level of E_C at the L point and the X_4 level of the HH level to the X_1 level of E_C at the X point.[30] E_1 ($\equiv L_1 - L_{3'}$) and E_2 ($\equiv X_1 - X_4$) are the energy gaps at the L and X points, respectively.

entire crystal direction, the peak I_{PL} parallel to $\boldsymbol{E}_I$ is higher than that perpendicular to $\boldsymbol{E}_I$. The P properties are consistent with the reference results of the Si quantum well structures at $E_{PH} \approx 1.7$ eV.[18] Consequently, the E_G values obtained by the PL method are isotropic in the entire crystal direction in the 2D Si plane.

3.4 Reflectivity modulation of 2D-SOQ

In Sect. 3.2, we demonstrated the BSM at the Γ point by showing the PL results. In this subsection, we discuss the BSM besides the Γ point by showing the R modulation of 2D-SOQ in the UV region.

Figure 7 shows a schematic band diagram of 3D-Si.[30] Using high energy photons in the UV region, electrons of heavy hole bands (HH) can directly transit to the conduction bands. The energy gaps at the L and X points are E_1 and E_2, respectively, where the reflectivity and absorptance of photons have the peak values at both E_1 and E_2 photon energies.[30] On the other hand, there is no reflectivity and absorptance peaks at the Γ point (E_0), because of the low density of states at the Γ point.[30]

Figure 8(a) shows the R spectra of 2D-SOQ in the UV region at various T_S values. Arrows show the E_1 and E_2 peaks of photons that correspond to the direct transmission from the valence band to the conduction band at the L and X points shown in Fig. 7. Namely, Fig. 7 shows that $E_1 \equiv L_1 - L_{3'}$ and $E_2 \equiv X_1 - X_4$, where L_1 and $L_{3'}$ are energy levels of the conduction and HH bands at the L point, and X_1 and X_4 are energy levels of the conduction and HH bands at the X point, respectively.[30] When $T_S > 4.8$ nm, E_1 and E_2 peaks are clearly observed. However, with decreasing T_S, E_1 and E_2 peaks become unclear, and E_1 and E_2 values shift, suggesting that the energy band structures of the 2D-SOQ are also modulated in the L and X points at $T_S \leq 1.9$ nm.

To analyze the T_S dependence of E_1 and E_2, Fig. 8(b) shows $(dR/dE)/R$ as a function of photon energy $E = h\nu$. E_1 and E_2 values can be obtained using $(dR/dE)/R = 0$ and are shifted by decreasing T_S. Here, Fig. 8(c) shows the T_S dependences of E_1 and E_2. With decreasing T_S, E_1 increases, but E_2 decreases, resulting in $E_1 \approx E_2$ at T_S of around 1 nm. As a result, the E_1 and E_2 shifts become larger than 0.5 eV with decreasing T_S from 50 to 1 nm. Therefore, the R properties of 2D-SOQ also suggest the energy-band structure modulation even in the other wave vector region besides the Γ point in the 2D Si layer.

4. Conclusions

We experimentally verified a crystal direction dependence of quantum confinement effects, such as the modulation of phonon spectra and the energy band structures of (100) 2D Si layer on silicon-on-quartz (SOQ) without a handle Si substrate under the BOX layer, using polarization Raman and PL methods. The polarization laser angle ϕ dependence of the first-order Raman intensity at the Γ point (520 cm^{-1}) obeys the Raman selection rule (RSR) even in 1-nm-thick 2D Si layer. However, for the first time, we demonstrated that the Raman intensity in the phonon confinement effects (PCEs) region of 480 cm^{-1} relaxes the RSR, which is attributable to the relaxed momentum conservation of the phonon wave vector $\boldsymbol{q}$ caused by Heisenberg's uncertainty principle of $\boldsymbol{q}$.

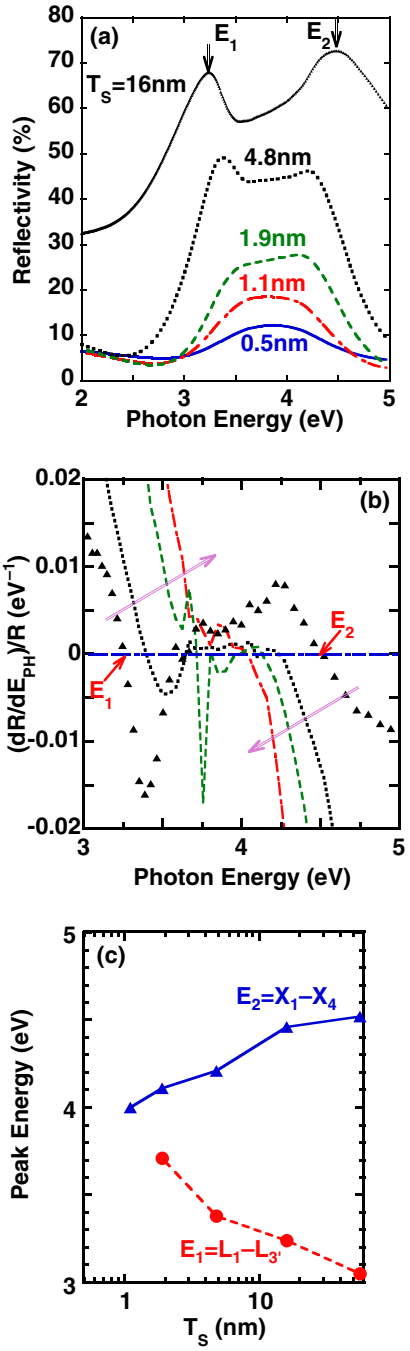

Fig. 8. (Color online) (a) UV reflectivity R spectra of SOQ with various T_S values. Although E_1 and E_2 peaks (arrows) are clearly observed at larger T_S values, E_1 and E_2 become unclear with decreasing T_S. (b) $(dR/dE_{PH})/R$ versus photon energy, which is evaluated from (a) data. E_1 and E_2 values, which are obtained using $(dR/dE_{PH})/R = 0$, are shifted by decreasing T_S. (c) E_1 and E_2 obtained using (b) as a function of T_S. With decreasing T_S, E_1 increases, E_2 decreases, and thus E_1 becomes nearly equal to E_2 at $T_S \approx 1$ nm.

On the other hand, the photon peak energy E_{PH} obtained by the PL method, that is, the bandgap energy E_G of the 2D Si layer, is isotropic in the entire crystal direction at the 2D Si layer surface, owing to the fact that quantum confinement effects of electrons are induced only at the direction perpendicular to the 2D-Si plane. In addition, the PL intensity parallel to the incident laser is higher than that perpendicular to the incident laser, and thus, the PL intensity is polarized. However, the PL polarization at $E_{PH} = 1.69$ eV is very small (0.052) in the entire crystal direction of the 2D Si layer.

Moreover, the reflectivity of the 2D Si layer in the UV region is also modulated. The reflectivity property modulation is possibly attributable to the energy band modulation besides the Γ point in the 2D Si layer.

Consequently, it is necessary to reconstruct the device design for CMOS composed of 2D Si structures, such as ETSOIs and FinFETs, considering the quantum mechanical confinements of phonon spectra and the energy band modulation in the 2D Si layer.

Acknowledgement

This work was partially supported by a Grant-in-Aid for Scientific Research from the Japan Society for the Promotion of Science (24560422).

1) A. Nazarov, J.-P. Colinge, F. Balestra, J.-P. Raskin, F. Gamiz, and V. S. Lysenko, *Semiconductor-On-Insulator Materials for Nanoelectronics Applications* (Springer, Berlin, 2011).
2) S. Saito, D. Hisamoto, H. Shimizu, H. Hamamura, R. Tsuchiya, Y. Matsui, T. Mine, T. Arai, N. Sugii, K. Torii, S. Kimura, and T. Onai, Jpn. J. Appl. Phys. **45**, L679 (2006).
3) S. Saito, N. Sakuma, Y. Suwa, H. Arimoto, D. Hisamoto, H. Uchiyama, J. Yamamoto, T. Sakamizu, T. Mine, S. Kimura, T. Sugawara, M. Aoki, and T. Onai, IEDM Tech. Dig., 2008, 19.5.
4) T. Mizuno, N. Sugiyama, T. Tezuka, Y. Moriyama, S. Nakaharai, and S. Takagi, IEEE Trans. Electron Devices **52**, 367 (2005).
5) T. Mizuno, N. Sugiyama, T. Tezuka, T. Numata, and S. Takagi, IEEE Trans. Electron Devices **50**, 988 (2003).
6) K. Uchida, H. Watanabe, A. Kinoshita, J. Koga, T. Numata, and S. Takagi, IEDM Tech. Dig., 2002, p. 47.
7) K. Uchida, J. Koga, and S. Takagi, J. Appl. Phys. **102**, 074510 (2007).
8) G. Tsutsui, M. Saitoh, and T. Hiramoto, IEEE Electron Device Lett. **26**, 836 (2005).
9) B. K. Agrawal and S. Agrawal, Appl. Phys. Lett. **77**, 3039 (2000).
10) M. Tabe, M. Kumezawa, and Y. Ishikawa, Jpn. J. Appl. Phys. **40**, L131 (2001).
11) Z. H. Lu and D. Grozea, Appl. Phys. Lett. **80**, 255 (2002).
12) N. Fukata, T. Oshima, N. Okada, K. Murakami, T. Kizuka, T. Tsurui, and S. Ito, J. Appl. Phys. **100**, 024311 (2006).
13) K. W. Adu, H. R. Gutierrez, and P. C. Eklund, in *Nanosilicon*, ed. V. Kumar (Elsevier, Amsterdam, 2008) Chap. 7.
14) H. Richter, Z. P. Wang, and L. Ley, Solid State Commun. **39**, 625 (1981).
15) I. H. Campbell and P. M. Fauchet, Solid State Commun. **58**, 739 (1986).
16) L. Khriachtchev, M. Räsänen, S. Novikov, O. Kilpelä, and J. Sinkkonen, J. Appl. Phys. **86**, 5601 (1999).
17) G. Faraci, S. Gibilisco, P. Russo, A. R. Pennisi, and S. La Rosa, Phys. Rev. B **73**, 033307 (2006).
18) S. Piscanec, M. Cantoro, A. C. Ferrari, J. A. Zapien, Y. Lifshitz, S. T. Lee, S. Hofmann, and J. Robertson, Phys. Rev. B **68**, 241312(R) (2003).
19) L. Donetti, F. Gámiz, J. B. Roldán, and A. Godoy, J. Appl. Phys. **100**, 013701 (2006).
20) T. Mizuno, K. Tobe, Y. Maruyama, and T. Sameshima, Jpn. J. Appl. Phys. **51**, 02BC03 (2012).
21) T. Mizuno, T. Aoki, Y. Nagata, Y. Nakahara, and T. Sameshima, Jpn. J. Appl. Phys. **52**, 04CC13 (2013).
22) S. S. Iyer and Y.-H. Xie, Science **260**, 40 (1993).
23) K. Mizoguchi and S. Nakashima, J. Appl. Phys. **65**, 2583 (1989).
24) T. Mizuno, Y. Nagata, Y. Suzuki, Y. Nakahara, T. Tanaka, T. Aoki, and T. Sameshima, Ext. Abstr. Solid State Devices and Materials, 2013, p. 96.
25) T. Tada, V. Poborchii, and T. Kanayama, J. Appl. Phys. **107**, 113539 (2010).
26) Web [http://www.shinetsu.co.jp/en/].
27) Web [http://www.soitec.com/en/].
28) Y. Kanemitsu and S. Okamoto, Phys. Rev. B **56**, R15561 (1997).
29) D. Kovalev, M. Ben Chorin, J. Diener, F. Koch, Al. L. Efros, M. Rosen, N. A. Gippius, and S. G. Tikhodeev, Appl. Phys. Lett. **67**, 1585 (1995).
30) J. R. Chelikowsky and M. L. Cohen, Phys. Rev. B **14**, 556 (1976).